remote sensing

MDPI

Article

Analyzing Spatiotemporal Variations and Driving Factors of Grassland in the Arid Region of Northwest China Surrounding the Tianshan Mountains

Yutong Fang [1,2], Xiang Zhao [1,2,*], Naijing Liu [3], Wenjie Zhang [1,2] and Wenxi Shi [1,2]

1 State Key Laboratory of Remote Sensing Science, Faculty of Geographical Science, Beijing Normal University, Beijing 100875, China; fangyutong@mail.bnu.edu.cn (Y.F.); zhangwenjie@mail.bnu.edu.cn (W.Z.); wenxi_shi@mail.bnu.edu.cn (W.S.)
2 Beijing Engineering Research Center for Global Land Remote Sensing Products, Faculty of Geographical Science, Beijing Normal University, Beijing 100875, China
3 POWERCHINA Northwest Engineering Corporation Limited, Xi'an 710065, China; liunj@mail.bnu.edu.cn
* Correspondence: zhaoxiang@bnu.edu.cn; Tel.: +86-010-5880-0181

Abstract: The Tianshan Mountains, the largest arid mountain range in Central Asia, feature diverse terrains and significant landscape heterogeneity. The grasslands within the Xinjiang Tianshan region are particularly sensitive to climate change and human activities. However, until recently, the patterns and mechanisms underlying grassland changes in this region have been unclear. In this study, we analyzed spatial and temporal changes in grassland fractional vegetation cover (FVC) from 2001 to 2020, analyzed spatial and temporal changes in grassland, and predicted future trends using Global Land Surface Satellite (GLASS) FVC data, trend analysis, and the Hurst index method. We also explored the driving mechanisms behind these changes through the structural equation model (SEM). The results showed that from 2001 to 2020, the grassland FVC in the Tianshan region of Xinjiang was higher in the central and western regions and lower in the northern and southern regions, showing an overall fluctuating growth trend, with a change in the growth rate of 0. 0017/a ($p < 0.05$), and that this change was spatially heterogeneous, with the sum of significant improvement (20.6%) and slight improvement (29.9%) being much larger than the sum of significant degradation (0.6%) and slight degradation (9.5%). However, the Hurst index (H = 0.47) suggests that this trend may not continue, and there is a risk of degradation. Our study uncovers the complex interactions between the Tianshan barrier effect and grassland ecosystems, highlighting regional differences in driving mechanisms. Although the impacts of climatic conditions in grasslands vary over time in different regions, the topography and its resulting hydrothermal conditions are still dominant, and the extent of the impact is susceptible to fluctuations of varying degrees due to extreme climatic events. Additionally, the number of livestock changes significantly affects the grasslands on the southern slopes of the Tianshan Mountains, while the effects of nighttime light are minimal. By focusing on the topographical barrier effect, this study enhances our understanding of grassland vegetation dynamics in the Tianshan Mountains of Xinjiang, contributing to improved ecosystem management strategies under climate change.

Keywords: Tianshan Mountains; grasslands; driving factors; structural equation model; climate change

Citation: Fang, Y.; Zhao, X.; Liu, N.; Zhang, W.; Shi, W. Analyzing Spatiotemporal Variations and Driving Factors of Grassland in the Arid Region of Northwest China Surrounding the Tianshan Mountains. *Remote Sens.* **2024**, *16*, 1952. https://doi.org/10.3390/rs16111952

Academic Editors: Hooman Latifi, Nikos Koutsias and Hamed Naghavi

Received: 13 April 2024
Revised: 20 May 2024
Accepted: 27 May 2024
Published: 29 May 2024

1. Introduction

Grasslands, which connect the lithosphere, pedosphere, atmosphere, hydrosphere, and biosphere, are critically important ecosystems in arid and semi-arid regions, covering 88% of the area [1,2]. They play a crucial role in biodiversity conservation, carbon cycling, and climate regulation [3,4]. Fractional vegetation cover—the ratio of the vertically projected vegetation area to the total ground area [5]—is extensively utilized to identify trends in grassland cover changes and climate variability [6]. It reflects the density, growth status,

and photosynthetic area of vegetation [7] and serves as a crucial indicator for assessing vegetation distribution, coverage, and ecological development, especially in the context of significant global changes [8,9]. Investigating the shifts in grassland cover and their climatic influencers is essential for comprehending grassland ecosystem functionalities and promoting sustainable development [10].

The spatial and temporal dynamics of grasslands in the Tianshan Mountains are complex, driven by both natural factors and human activities [11–13]. Previous studies have demonstrated that the Tianshan Mountains, situated in a transition zone and highly sensitive to diverse environmental changes [14,15], exhibit significant variations in grass cover across different areas [16–18]. Grasses on the western side of the Tianshan Mountains exhibit better growth, yet the extent of degradation is more pronounced [19]. In terms of climate, water scarcity is a major limiting factor affecting vegetation dynamics, and reduced precipitation coupled with a warming climate can lead to soil droughts and exacerbate the deterioration of the condition of grassland vegetation [20–22]. Interestingly, warming has sometimes mitigated some of the negative impacts on the ecosystems of the region, as snowmelt from March to May has increased soil moisture, contributing to the recovery of grasslands in the Tianshan Mountains region [23]. As one of the grassland bases for livestock production in China, overgrazing in the Tianshan Mountains may lead to a decrease in grassland cover [24,25], whereas moderate grazing may improve grassland cover, productivity, and biodiversity. Additionally, human interventions, such as diversifying water resources from mountains to oases for economic and social development, may reduce the ecological water supply, worsening ecological imbalances [26]. Therefore, these factors must be collectively considered to gain a deeper understanding of the growth dynamics of the Tianshan Mountains grasslands.

The distribution of grassland cover is intricately linked to an area's topography. There is growing evidence suggesting that topography has a significant impact on water and heat exchange between soil, air, and plants, as well as on human activities [10,27,28]. For example, in Bangladesh's Chittagong Hill Tracts, Emran demonstrated a strong correlation between the normalized difference vegetation index (NDVI) and topographic variables [29]. However, traditional analytical methods usually only investigate the direct effects of environmental or anthropogenic factors on vegetation dynamics [30]. Research on the driving factors behind the differences in grassland distribution between the northern and southern slopes of the Tianshan Mountains is limited; this oversight leads to an incomplete understanding of the complex spatial differentiation of the Tianshan grasslands. It is necessary to quantify the interactions between the topography and other influences to more fully understand the spatial and temporal patterns of grassland forest cover and to decipher their underlying drivers.

The Tianshan Mountains, often referred to as the "Water Tower of Central Asia" [31], connect the Junggar and Tarim basins and support the largest ecosystems in the arid Central Asian landscape [32]. In recent decades, with the deterioration of climate change due to rising global temperatures and frequent extreme weather events, this ecosystem has been increasingly threatened by the rapidly developing regional economy and urbanization, as evidenced by the continuous decline in productivity and environmental problems [33]. In 2015, grassland vegetation coverage was recognized as a critical metric for evaluating the ecological civilization progress [34]. Therefore, given the pivotal role of grassland resources in Xinjiang's economic and social fabric [35], a full understanding of grassland changes is a prerequisite for promoting sustainable ecological and environmental developments in Xinjiang.

The response and adaptive capacity of grassland ecosystems to environmental changes in the Tianshan Mountains of Xinjiang have garnered attention in the fields of ecology and environmental science. This study aims to delve into the following scientific questions: (1) How have the spatial and temporal dimensions of grassland FVC in Xinjiang changed over the last 20 years? (2) Has the response of grassland ecosystems to changing environmental conditions evolved? To address these questions, we described the spatial and

temporal distribution patterns and future evolutionary trends of grassland resources in Xinjiang from 2001 to 2020, and further studied the actual impact of these factors on the grassland ecosystem. The findings of this study will serve as a fundamental reference for comprehensively understanding Xinjiang grasslands and their management. Moreover, they will provide a theoretical basis for evaluating the regional ecological environment and guiding land use planning and ecological decision-making processes.

2. Materials and Methods

2.1. Study Area

The Tianshan Mountains, recognized as one of the seven major mountain ranges of the world, are the most expansive within the global temperate arid zone and the most remote from any ocean [36,37]. Our research zeroes in on the Tianshan Mountains' eastern section, specifically the Xinjiang Tianshan section (TS, 73°50′~95°33′E, 39°24′~45°23′N), nestled between the Junggar Basin to the south and the Tarim Basin to the north, spanning from Hami City in the east to the Ili River Basin in the west, across central Xinjiang. This area comprises three major mountains, over twenty mountain ranges, and more than ten intermountain basins or valleys (Figure 1). The Xinjiang Tianshan Mountains' intricate topography, arid climate, desert soils, and vegetation foster a rich tapestry of biological communities [38].

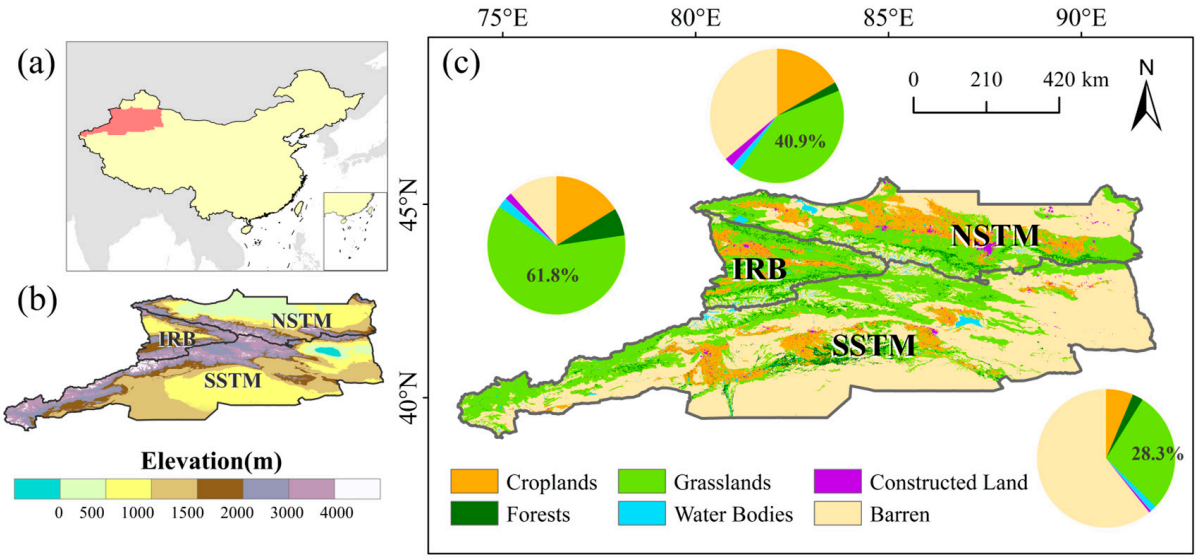

Figure 1. Map of the study area: (**a**) location of the study area in the whole of China; (**b**) spatial distribution of elevation in the study area. TS: Tianshan Mountains; NSTM: northern slope of the Tianshan Mountains; IRB: Ili River Basin; SSTM: southern slope of the Tianshan Mountains. (**c**) Land use coverage of the study area (2020), where pie charts show the percentage of area occupied by different land use types.

Deserts flank both the north and south sides of these mountains, leading to marked climatic, soil, and vegetation coverage variations between the Ili River (west side) and the northern and southern flanks. Consequently, the Xinjiang Tianshan Mountains are divided into three subregions, reflecting their geographical and topographical distinctions: the northern slope of the Tianshan Mountains (NSTM), the Ili River Basin (IRB), and the southern slope of the Tianshan Mountains (SSTM).

2.2. Data and Processing

2.2.1. FVC Data

The GLASS FVC product is a remote sensing inversion product characterized by its extended time series, high resolution, and high precision, obtained through an inversion

algorithm using multi-source remote sensing data and measurement station data [39]. The data have spatial and temporal resolutions of 500 m and 8 days, respectively. The GLASS raw data, in HDF format, was batch converted to the GeoTIFF format using the MRT tool and then reprojected from a sinusoidal projection to a WGS_1984 projection. Subsequently, the GLASS FVC dataset for the growing season (April–October) from 2001 to 2020 was synthesized using averaging, which can reflect the status of vegetation growth records more comprehensively than the maximum value synthesis method, avoiding the impact of extreme climate anomalies on vegetation [40].

2.2.2. Climate Data

Meteorological data for this research were sourced from the ERA5_Land reanalysis datasets, disseminated by the European Center for Medium-Range Weather Forecasts (ECMWF). ERA5-Land, the terrestrial segment of the ERA5 climate reanalysis, offers hourly updates on high-resolution surface variables, with a temporal resolution of 1 h and a spatial resolution of $0.1^\circ \times 0.1^\circ$. Notably, this dataset is renowned for its finer spatial resolution and superior performance in Central Asia [41]. In this study, we focused on three meteorological variables: surface 2 m temperature, precipitation, and net solar radiation. The mean temperature and solar radiation were derived by averaging these variables across the growing season from April–October. Similarly, total precipitation was computed by aggregating rainfall amounts for the same period.

2.2.3. Socioeconomic Data

The livestock data were obtained from the 2001–2020 Statistic Bureau of the Xinjiang Uygur Autonomous Region and related literature, which then were collated. The nighttime light index was derived from an extended time series of cross-sensor calibrated global NPP-VIIRS nighttime light data (2001–2020) [42]. Population data were obtained from the WorldPop Global Project Population Data, a dataset of residential population density on a 100×100 m grid.

2.2.4. Additional Data

The digital elevation model (DEM) utilized in this study is sourced from the Shuttle Radar Topography Mission (SRTM) product, made available by the United States Geological Survey (USGS) data center, featuring a spatial resolution of 30 m. For the land use analysis, the MODIS land cover product MCD12Q1 V6 was employed. This dataset categorizes the Earth's surface into six global land cover types, utilizing various classification schemes, all at a spatial resolution of 500 m. The adoption of this high-quality, detailed dataset is pivotal for ensuring precise and accurate terrain and land-use analysis and mapping.

2.2.5. Data Processing

To ensure that the spatial resolution of topographic and meteorological data was consistent with that of remote sensing image data, ArcGIS 10.2 software was used to resample the data to a 500 m resolution through projection conversion and mosaicking tools. Socioeconomic data were statistically recorded according to county-level administrative divisions. Due to the differences in the herbivory of different livestock, they were uniformly converted to sheep units in this study, and then further converted to raster images, which were finally resampled to 500 m raster images. The fixed grassland pixels in the Xinjiang region for the years 2001–2020 were captured pixel-by-pixel through the land-use data, and the vector data of Xinjiang's grassland coverage were generated.

2.3. Study Method

2.3.1. Linear Regression

To calculate the overall trend of the year-to-year growing season mean values of FVC of grassland vegetation in the Tianshan Mountains and its subregions, this study was carried out by establishing a linear regression model. The calculation formula is as follows:

$$Slope = \frac{n\sum_{i=1}^{n} i \times X_i - \sum_{i=1}^{n} i \sum_{i=1}^{n} X_i}{n\sum_{i=1}^{n} i^2 - \left(\sum_{n}^{i=1} i\right)^2}, \quad (1)$$

where slope denotes the slope of change; X_i denotes the variable of the i-th value, and n is the cumulative number of years in the study period.

2.3.2. Theil–Sen Median Trend Analysis and Mann–Kendall Test

The spatial trend of grassland in Xinjiang was investigated using a combination of Theil–Sen trend analysis and the Mann–Kendall test method. Firstly, the Theil–Sen method was employed to calculate the trend of grassland resources on an image-by-image metric basis [43,44], which is a robust trend calculation method with low data requirements, and which is insensitive to noise and outliers, and which can be better used for long time series analysis [45]. Its calculation formula is:

$$\beta = median\frac{x_j - x_i}{j - i}, 1 < i < j < n \quad (2)$$

where β refers to the Theil–Sen median; x_i and x_j denote the values corresponding to years i and j. When $\beta > 0$, this indicates that the time series shows a growing trend; the opposite result represents a degrading trend.

The Mann–Kendell test, a commonly used mutation detection method, is a distribution-free test method in which the selected samples do not need to obey the positive distribution [46,47], offer the advantage of simple calculation, are unaffected by missing values and outliers, and reflect the long-term trend of the sample and the mutation [48]. The calculation formula is as follows:

$$S = \sum_{i=1}^{n-1} \sum_{j=i+1}^{n} \mathrm{sgn}(x_j - x_i), \quad (3)$$

where n is the length of the time series, and x_i and x_j denote the value of the image element in years i and j, respectively. The symbolic function sgn ( ) is given by:

$$\mathrm{sgn}(x_j - x_i) = \begin{cases} 1\ (x_j - x_i > 0) \\ 0\ (x_j - x_i = 0) \\ -1\ (x_j - x_i < 0) \end{cases}, \quad (4)$$

The variance of S is:

$$Var(S) = \frac{n(n-1)(2n-5)}{18}, \quad (5)$$

If the sample number $n > 10$, the standardized statistic Z is calculated as:

$$Z = \begin{cases} \frac{S-1}{\sqrt{Var(S)}}, S > 0 \\ 0, S = 0 \\ \frac{S+1}{\sqrt{Var(S)}}, S < 0 \end{cases} \quad (6)$$

Z obeys the normal distribution. When $|Z| > Z_{1-\alpha/2}$, the sequence is said to be significant at the α level.

2.3.3. Hurst Index

The Hurst index can quantitatively describe the self-similarity and long-term correlation of time series data [49], and it is widely used in research fields such as climatology and geology [50]. To analyze the future trend change of grassland resources, the Hurst index was introduced for analysis, based on the rescaled range (R/S) theory, and the main calculation steps are as follows:

(1) Define a time series: $\{V(\tau)\}$ (τ = 1, 2, 3, ... n), which is divided into τ subsequences $X(t)$, for each subsequence $t = 1, \ldots, \tau$.

(2) Define the average sequence of the long time series:

$$\overline{V_{(\tau)}} = \frac{1}{\tau}\sum_{t=1}^{r} V_{(t)}, \tau = 1,\ 2,\ 3,\ \ldots n \tag{7}$$

(3) Calculate the cumulative deviation from the mean of each time series V:

$$X_{(t,\tau)} = \sum_{u=1}^{t}\left(V_{(u)} - \bar{V}_{(\tau)}\right), 1 \le t \le \tau \tag{8}$$

(4) Define the sequence of the value fields of R:

$$R_{(\tau)} = \max_{1\leqslant t\leqslant \tau} V_{(t,\tau)} - \min_{1\leqslant t\leqslant \tau} V_{(t,\tau)}, \tau = 1,\ 2,\ 3, \ldots n \tag{9}$$

(5) Define the sequence of standard deviations of S:

$$S_{(\tau)} = \sqrt{\frac{1}{\tau}\sum_{t=1}^{\tau}\left[V_{(t)} - \overline{V_{(\tau)}}\right]^2}, \tau = 1,\ 2,\ 3, \ldots n \tag{10}$$

(6) Calculate the Hurst index (H):

$$(c\tau)^H = \frac{R_{(\tau)}}{S_{(\tau)}}, \tag{11}$$

The range of H value is 0 to 1; when $0 < H \le 0.5$, it means that the time series exhibits anti-sustainability and is a random sequence, and the closer H is to 0, the stronger the anti-sustainability; when $0.5 < H < 1$, it means that the time series is characterized by a long-term correlation and has the sustainability, and the closer H is to 1, the stronger the sustainability.

2.3.4. Pearson Correlation

To quantify the correlation between grassland changes and the influencing factors, this study employed the Pearson correlation coefficient method to quantitatively analyze the relative contribution of topographic, climatic, and anthropogenic factors to grassland changes. In this study, the correlation between FVC values and influencing factors was calculated on the Matlab platform, and the formula for the correlation coefficient was as follows:

$$r_{xy} = \frac{\sum_{i=1}^{n}(x_i - x)(y_i - y)}{\sqrt{\sum_{i=1}^{n}(x_i - \overline{x})^2 \sum_{i=1}^{n}(y_i - \overline{y})^2}}, \tag{12}$$

where r_{xy} represents the correlation coefficient between x and y, n represents the length of the time series; x_i represents the observed values, and y_j represents the observed values of the influencing factors. When $r_{xy} > 0$, it means that the variables are positively correlated; when $r_{xy} < 0$, the variables show a negative correlation; the closer the value of $|r_{xy}|$ is to 1, the higher the correlation between the factors.

2.3.5. Structural Equation Model

The structural equation model (SEM) is a statistical method based on the covariance matrix of variables used to analyze the relationship between variables [51,52]. Typically, assumptions about the relationships between variables are made based on a literature review or a priori knowledge. The model's fit is then assessed using fit optimality indices. If the model fits poorly, it may need to be reset, based on theoretical assumptions and statistical results, or insignificant paths may need to be deleted or changed to improve the fit of the SEM and explain the relationships between variables [53]. To determine the best-fit model, four metrics are selected: the CFI (comparative fit index), AGFI (adjusted goodness of fit index), RMSEA (root mean square error of approximation), and SRMR (standardized root mean square residual) [30]. Generally, a CFI and AGFI closer to 1, and an RMSEA and SRMR closer to 0 indicate a better model fit.

In this study, a structural equation model was built based on previous theories and a priori knowledge to investigate the influence of factors such as climate, topography, and human activities on grassland changes in Xinjiang. The maximum likelihood method was used for analysis. The model construction, evaluation, and correction were carried out in IBM SPSS Amos 26 software, part of the SPSS (Statistical Product Service Solutions) statistical package. The final fitted SEM is obtained when the model's goodness-of-fit metrics are met. Each path provides corresponding standardized regression coefficients. The direct effect is the coefficient of the path from the independent variable directly to the dependent variable; the larger the coefficient, the larger the effect. The indirect effect is the product of the coefficient of the path from the independent variable to the intermediate variable and the coefficient of the path from the intermediate variable to the dependent variable; if multiple intermediate variables exist, the indirect effect is the sum of each indirect effect. The total effect is the sum of the direct and indirect effects.

3. Results

3.1. Spatial and Temporal Patterns of FVC during the Growing Season

From 2001 to 2020, the FVC of grasslands in the Xinjiang Tianshan Mountains during the growing season exhibited a gradual increase from the northern and southeastern regions towards the central and western areas, as depicted in Figure 2a. This spatial pattern of grassland vegetation, characterized by its patchiness and discontinuity, is strongly influenced by the terrain. Specifically, lower grassland coverage tends to occur in low-altitude plains, whereas higher coverage is prevalent in mountainous regions. The FVC values for the grasslands range from 0 to 0.98, averaging 0.217. Pixels with FVC values exceeding the average represent 63.7% of the total, while those below the average account for 36.3%. FVC was divided into five categories: very low cover (0–0.2), low cover (0.2–0.4), medium cover (0.4–0.6), high cover (0.6–0.8), and very high cover (0.8–0.1) to reflect the growth status of grassland (Figure 2b). The results showed that the north and south slopes of the Tianshan Mountains were dominated by low cover grassland, accounting for 72.8% and 65.53% of the total area, respectively, and there was almost no high cover grassland. The overall vegetation cover of IRB during the growing season was higher, and the coverage of very high and high coverage grassland was 24.46% and 18.65%, respectively.

FVC in the grasslands of the Xinjiang Tianshan Mountains from 2001 to 2020, depicted in Figure 3, illustrates varying FVC trends across the region and its subregions. Box plots for the entire area and three specific subregions during this period (Figure 3a) reveal marked regional disparities in FVC. All regions except the Ili River Basin passed the significance threshold (p-value < 0.05). Figure 3b indicates that the overall grassland FVC trend in the Xinjiang Tianshan Mountains is characterized by significant variances and a marginal annual increase of 0.0017. The peak FVC value was 0.13 in 2019, with the lowest at 0.09 in 2001, showing a significant dip in 2014. Regional analysis (Figure 3c–e) shows that the Ili River Basin's grasslands exhibited the highest FVC over the two decades, averaging 0.49, while the southern slope's grasslands showed the lowest, with an average FVC of just 0.05. The FVC trends on the northern and southern slopes mirror the general pattern observed

across the Tianshan grasslands. However, the Ili River Basin's trend diverges significantly from that of the northern slope. In general, the FVC of the Tianshan Mountains and its subregions showed an upward trend, and the north slope of the Tianshan Mountains was the most obvious. The FVC fitting in the Ili River Basin has the smallest upward trend, and the reliability of the fitting curve is poor because of the large variance.

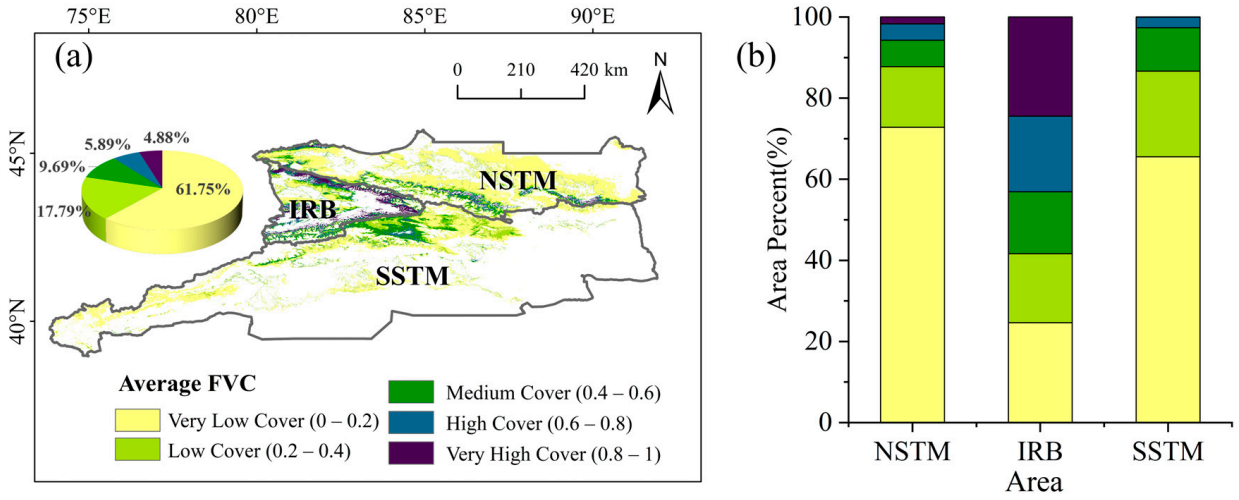

Figure 2. Spatial distribution pattern of grassland FVC during the growing season in the Tianshan Mountains of Xinjiang from 2001 to 2020. (**a**) Spatial distribution of mean values; (**b**) statistical results of the percentage of area occupied by grass FVC cover classes in different regions. The legend of (**b**) is the same as that of (**a**).

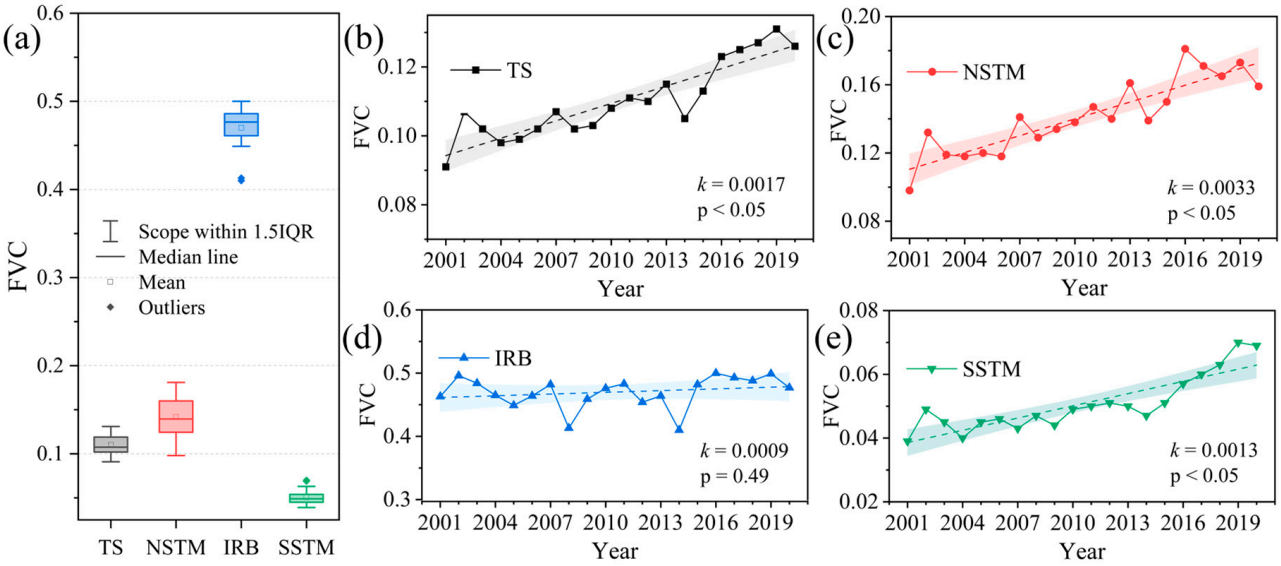

Figure 3. Interannual trends of FVC in growing season grasslands in the Tianshan Mountains, Xinjiang, 2001–2020. (**a**) Distribution of FVC values in the study area and its subregions, with boxes, whiskers, bars, and squares showing the range, maximum and minimum, median, and mean of FVC values, respectively; and plots of the interannual trends of grassland FVC in the four regions of TS (**b**), NSTM (**c**), IRB (**d**), and SSTM (**e**).

3.2. Trend Analysis of FVC during the Growing Season

Based on the Theil–Sen trend analysis and Mann–Kendell significance test, pixel-by-pixel calculations of grassland FVC from 2001 to 2020 were conducted, effectively expressing the spatial details of FVC evolution in the Xinjiang Tianshan Mountains from 2001 to 2020

(Figure 4a), and the results were divided into five change types (Table 1). From 2001 to 2020, the overall FVC of the Xinjiang Tianshan Mountains showed an improving trend, with 20.6% of the area significantly improved, 29.9% slightly improved, 39.4% remaining unchanged, 9.5% slightly degraded, and only 0.6% severely degraded, while also revealing clear regional differences (Figure 4b). Looking at the area percentage of different trend change types in the three regions, both the northern and southern slopes of the Tianshan Mountains showed a larger proportion of improved grassland areas, with the southern slope showing the most improvement (area percentage of 63%), mainly distributed in the northern slope grasslands, which were primarily characterized by unchanged change types. In contrast, a large area of degradation was detected in the Ili River Basin, with the proportion of grasslands showing a degradation trend reaching 37%. The Ili River Basin is one of the regions showing the most drastic changes in grassland resources, which are closely related to climate change and human activities.

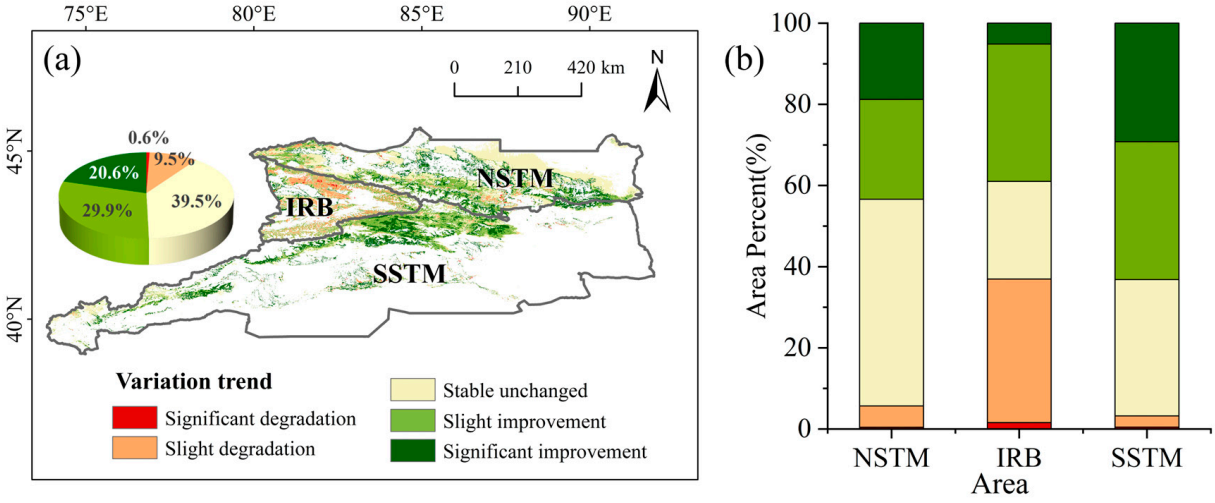

Figure 4. Trends in FVC of grassland in the Tianshan Mountains of Xinjiang during the growing season from 2001 to 2020. (**a**) Spatial trends of FVC; (**b**) statistical results of the percentage change of FVC in different regions. The legend of (**b**) is the same as that of (**a**).

Table 1. Trend analysis grading criteria.

Trends	S-Value	Z-Value
Significant degradation	$S \leq -0.0005$	$\|Z\| > 1.96$
Slightly degradation	$S \leq -0.0005$	$-1.96 \leq Z \leq 1.96$
Stable unchanged	$-0.0005 < S < 0.0005$	-
Slight improvement	$S \geq 0.0005$	$-1.96 \leq Z \leq 1.96$
Significantly improvement	$S \geq 0.0005$	$\|Z\| > 1.96$

The distribution of the Hurst index for the vegetation coverage of the Tianshan grasslands in Xinjiang is shown in Figure 5a, ranging from 0.08 to 1, with an average of 0.47. The area with a Hurst index of less than 0.5 accounts for 62% of the region, indicating that the FVC in the entire region shows weak anti-persistence, i.e., the change trend of FVC in the Tianshan grasslands may reverse after 2020, and there may be strong fluctuations in the future. To explore the future trend of FVC, we combined the Hurst index with the FVC trend (Figure 5b) and divided it into six change types (Table 2). The results (Figure 5c) show that the distribution of each change type occupies 3.8%, 6.6%, 20.6%, 31%, 14.8%, and 23.3% of the total area of Tianshan grasslands, respectively. The area with a declining trend in the future (34.8%) is larger than the area with an increasing trend (27.2%). Specifically, the largest proportion of the area in Tianshan that may change from improved to degraded in the future (ID) is widespread across the entire study area, while the smallest proportion

of the area that continues to degrade in the future (only 3.79%) is sporadically distributed nearby. The northern slope of Tianshan shows the largest area that may change from stability in the future (SC), the Ili River Basin also exhibits the largest area that may change from improvement to degradation in the future (ID), and the southern slope of Tianshan possesses the largest proportion of the area that continues to improve (II).

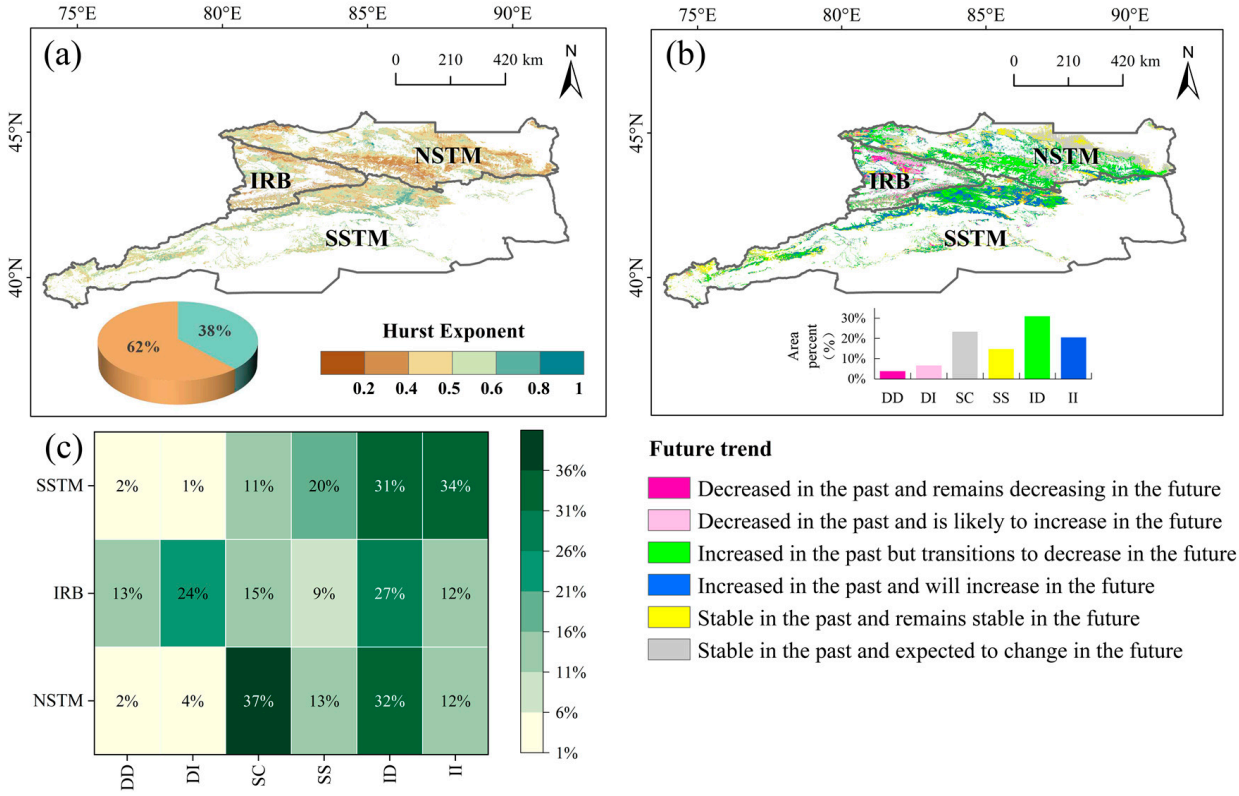

Figure 5. Future changes in FVC of growing season grassland in the Tianshan Mountains of Xinjiang from 2001 to 2020. (**a**) Spatial distribution map of the Hurst index, where the pie chart shows the proportion of the image area showing persistent and non-persistent changes; (**b**) spatial distribution map of consistency; and (**c**) area statistic results of the six trends of changes.

Table 2. Hurst index grading statistics.

Sen Slope	Hurst Index	Persistence of Future Change
$S \leq -0.005$	≥0.5	Decreasing in the past and continuing to decrease in the future (DD)
$S \leq -0.005$	<0.5	Decreasing in the past but may increase in the future (DI)
$-0.005 < S < 0.005$	≥0.5	Stable in the past and continuing to be stable in the future (SS)
$-0.005 < S < 0.005$	<0.5	Stable in the past but changing in the future (SC)
$S \geq 0.005$	≥0.5	Increasing in the past and continuing to increase in the future (II)
$S \geq 0.005$	<0.5	Increasing in the past but likely to decrease in the future (ID)

3.3. The Driving Factors of Vegetation Variations in the Tianshan Mountains

The spatial variation of FVC in the Tianshan grasslands is strongly correlated with environmental and climatic factors. Statistical analysis of the spatial distribution and inter-annual trends of precipitation, temperature, solar radiation, livestock number, nighttime light, and population density in the NSTM, IRB, and SSTM regions (Figure A1) revealed that the spatial distribution of the different influencing factors was heterogeneous: the NSTM region experienced significant urbanization and population expansion; the inter-annual variations of the environmental factors, such as precipitation and solar radiation, were large in the IRB region. In the SSTM region, the indicators are relatively stable.

To illuminate the complex dynamic interplay between grassland vegetation cover and a range of influencing factors across various subregions of the Tianshan Mountains, the SEM devised in this research meticulously explored the principal mechanisms driving vegetation cover across distinct watersheds. Given the stringent criteria of SEM for variable selection and sample size, a systematic exclusion of variables was conducted based on the correlation intensity among influencing factors and between the dependent variable and these factors. Initially, the analysis addressed the issue of multicollinearity among variables, subsequently eliminating the observed variables (population density) that exhibited weak correlations with changes in grassland vegetation (Figure A2). The fitting optimization indices of the ultimately established SEM model, which assessed the vegetation cover changes in the Tianshan grasslands, satisfied all specified criteria, affirming the model's robust alignment with the data.

Figure 6 delineates the dynamics of grassland vegetation cover on the northern slopes of the Tianshan Mountains from 2001 to 2020, illustrating that fluctuations in livestock numbers and nighttime light had a minimal influence on FVC. Conversely, precipitation and temperature exerted considerable direct impacts on the region's grassland vegetation cover, with coefficients of 0.23 and −0.41, respectively. Although the direct influence of topography on vegetation cover was slightly negative (−0.04), its indirect effects, mediated by climatic factors like precipitation and temperature, significantly bolstered its total effect to 0.48, establishing topography as the foremost determinant of vegetation cover in this locality. Subsequent analysis across the periods before and after 2010 (Figure A3) revealed a gradual decline in the contributions of topography and anthropogenic factors to the FVC, with topography expressing the most notable change, leading to a decrement of 0.063 in its overall effect. On the contrary, the negative effect of temperature was weakened. Notably, the impact of nighttime light shifted from an initially weak positive to a negative influence.

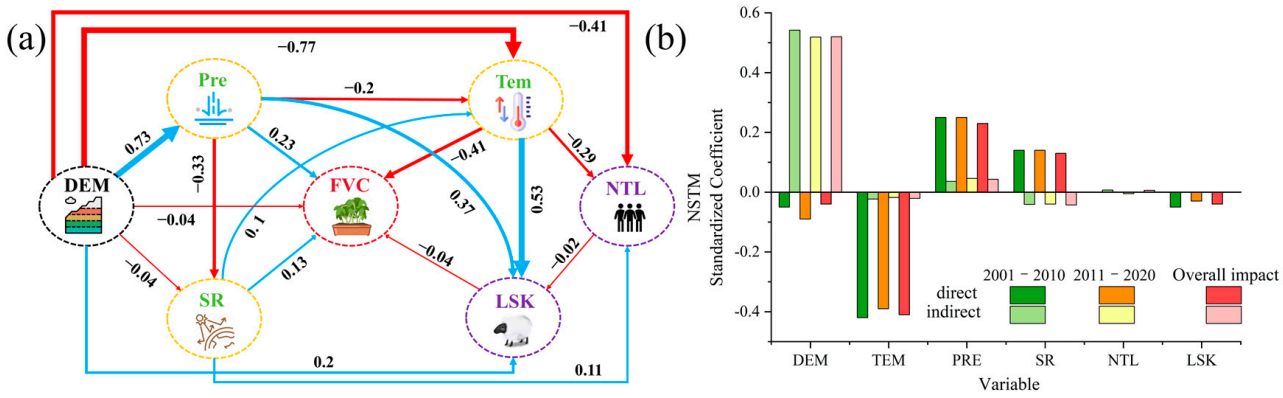

Figure 6. Structural equation model and contribution of FVC and influencing factors to the growing season of grasslands in the northern slope of Tianshan Mountains: (**a**) 2001–2020 and (**b**) standardized direct and indirect effect statistics. Abbreviations are the same as in Figure A2.

Figure 7 presents the outcomes of SEM conducted for the Ili River Basin, revealing temperature as the primary factor influencing FVC in the area, with a total effect coefficient of −0.52. Moreover, topography enhances this effect via its climatic impact, evidenced by a total effect coefficient of 0.276. This region exhibits a stronger correlation between nighttime light and FVC when compared to other Tianshan regions, suggesting that areas with increased lighting may be linked to ecological disruptions caused by human activities. From the initial to the latter decade, a progressive decline in the positive impacts of topography, precipitation, temperature, and live-stock numbers on FVC can be observed (Figure A4). Conversely, the beneficial effects of solar radiation and livestock numbers on vegetation cover showed only marginal enhancements. Unlike the effects on the northern slopes of the Tianshan Mountains, the influence of nighttime light on the IRB region transitioned from a negligible to a positive impact on vegetation cover.

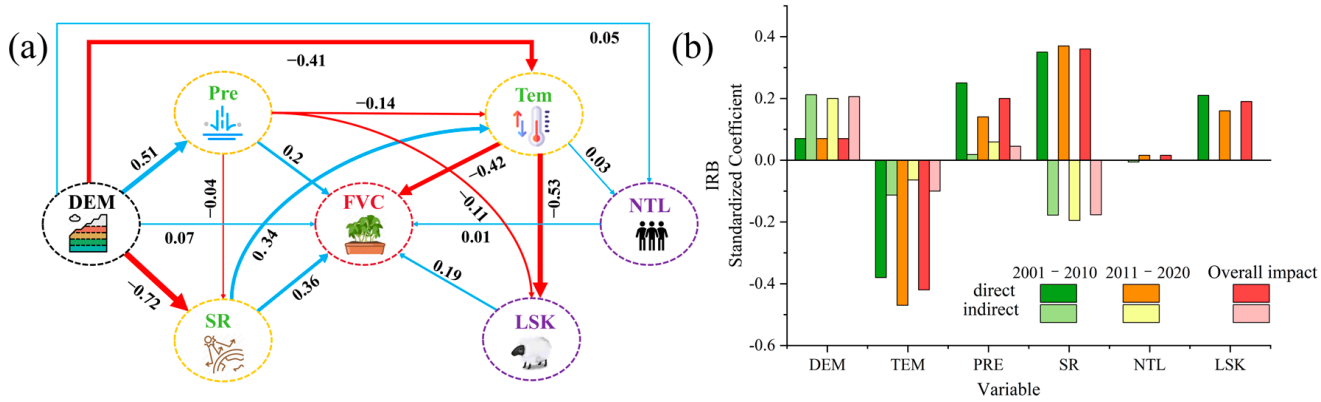

Figure 7. Structural equation model and contribution of FVC and influencing factors to the growing season of grasslands in the Ili River Basin: (**a**) 2001–2020 and (**b**) standardized direct and indirect effect statistics. Abbreviations are the same as in Figure A2.

Figure 8 illustrates the findings of SEM conducted on the southern slope of the Tianshan Mountains. The results reveal that, in addition to the significant effects of precipitation, temperature, and solar radiation, livestock density has a notable positive impact on FVC. This underscores the crucial role of sustainable livestock management practices in enhancing grassland vegetation cover in the region. While topography directly negatively affects vegetation cover, its indirect effect positively influences vegetation growth by mitigating the adverse effects of temperature increase (−0.72) and influencing human activities (−0.11). Precipitation emerges as the main positive factor influencing vegetation cover, with a coefficient of 0.455. Temporal analysis of the SEM decade reveals a diminishing positive effect of topography, precipitation, and livestock density on grassland vegetation (Figure A5).

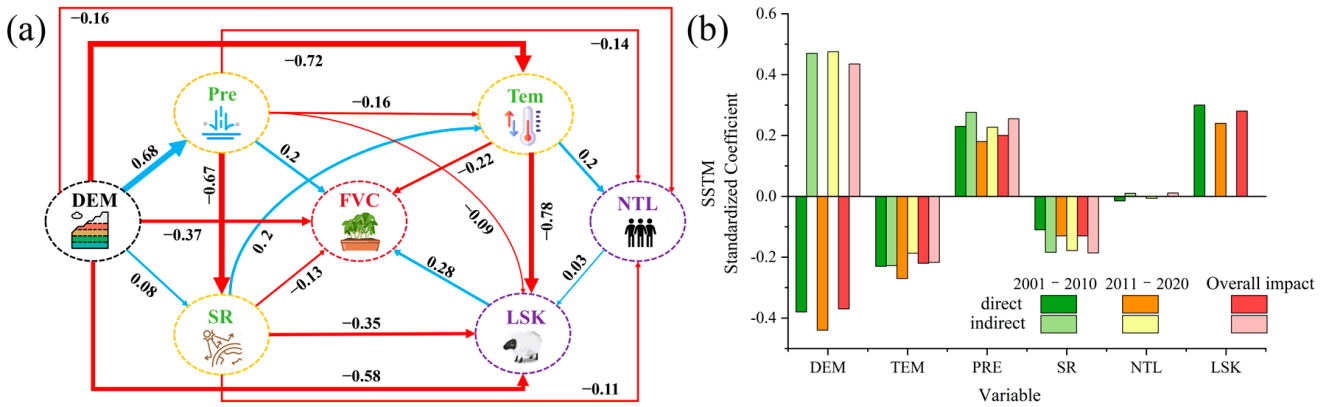

Figure 8. Structural equation model and contribution of FVC and influencing factors to the growing season of grasslands in the southern slope of Tianshan Mountains: (**a**) 2001–2020 and (**b**) standardized direct and indirect effect statistics. Abbreviations are the same as in Figure A2.

4. Discussion

4.1. Spatial Distribution and Variation of FVC during the Growing Season

This study utilized GLASS FVC data to analyze the spatiotemporal changes in grassland coverage in the Tianshan Mountains of Xinjiang over the past 20 years, predicting future trends. The observed distribution pattern of grassland FVC in the Tianshan region of Xinjiang aligns with that in Zhao's study [54], highlighting spatial heterogeneity characterized by high, medium, and low coverage along the elevation gradient. The primary source of moisture in the Tianshan Mountains is the Atlantic Ocean, with additional contributions from the Arctic Ocean, entering from the western mountainous regions of the Junggar Basin [37,55]. Therefore, the grasslands in the Ili River Basin are in good condition, while

the grassland coverage in the plains of the southern slope of the Tianshan Mountains is generally low. Low vegetation areas are predominantly found in ecologically sensitive and fragile regions, such as basin edges, where high temperatures, low rainfall, abundant sunlight, severe land desertification, and low water conservation capacity create harsh conditions for vegetation [56].

The Theil–Sen trend analysis and Mann–Kendell tests from 2001 to 2020 reveal a fluctuating increase in the FVC of the Tianshan grasslands, marked by overall improvement and localized degradation. About 50.5% of the area improved, while 10.1% degraded, aligning with the results of earlier remote sensing studies [57–59], and most of the degraded areas are located in the Ili River Basin [19]. Meteorological analysis indicates that since 2000, average temperatures and solar radiation in the region have slightly increased, while precipitation during the growing season has decreased [60]. This pattern reflects an "asymmetric warming–wetting" climate trend in Xinjiang since 2000, suggesting a regional tendency towards warmer, moister conditions, albeit with local warming and drying, and notable climatic oscillations [61]. Thus, Tianshan's FVC exhibits a fluctuating upward trend, with clear periodicity.

4.2. Analysis of Driving Factors of the FVC Spatial Pattern

The spatial distribution of grasslands in the Tianshan Mountains reflects a complex interplay of topography, climate, and human activities, significantly influenced by regional environmental variations [62]. Climate change, primarily through alterations in precipitation and temperature, further influences grassland growth and ecosystem productivity by modifying soil moisture and soil microbes, and by impacting photosynthesis and plant respiration [63,64]. The observed positive correlation between grassland FVC and precipitation and the negative correlation with temperature align with the findings of previous studies [38,54,65]. Xinjiang's location, far from the ocean, leads to limited moisture sources and scarce precipitation, comprises the core of China's arid region, characterized by desert vegetation, and a temperature rise enhances evaporation from the vegetation surface, which hinders the storage and use of water by vegetation, thus negatively impacting its growth and development [66], hence the negative correlation with FVC. Conversely, an increase in precipitation can effectively offset soil moisture deficits in arid and semi-arid regions, reduce surface evaporation, improve vegetation photosynthetic efficiency, and boost the accumulation of organic dry matter [67], acting as a catalyst for increased grassland coverage in the Tianshan region.

Many studies have shown that natural factors often interact rather than operate independently, and that the interaction between these factors enhances the explanatory power of grassland drivers. Prior modeling studies have indicated that indirect effects are more significant in arid regions than in humid areas [68,69]. In our study, SEM revealed that topographic variations and the consequent changes in water–heat conditions were identified as the primary factors affecting vegetation growth in the Xinjiang region [70,71]. Therefore, the discrepancy in moisture input caused by the mountains may result in notable differences in the arid climate of the northern and southern Tianshan Mountains, especially in terms of temperature, precipitation, and soil, thereby establishing a natural ecosystem in the plains consisting of alpine meadows, mid-mountain humid forests, semi-arid grasslands, and arid deserts [72]. The interception and lifting effect of mountains on water vapor amplifies and elevates the vertical movement and concentration of water vapor on the windward slope, which, with adequate water vapor supply, can lead to significant precipitation [73]. This blocking effect causes the Atlantic water vapor entering the western gap of the Junggar Basin to generate orographic rain, supplying ample water for vegetation growth; meanwhile, the southern slope, being leeward, with low rainfall and high evaporation, is marked by desert zones and sparse vegetation growth, especially in regards to grasslands [74].

Compared to hydrothermal conditions, changes in solar radiation have a less pronounced impact on grassland FVC. Solar radiation primarily influences vegetation growth

by affecting photosynthesis, microbial activity, and nutrient cycling in the soil. It also plays a crucial role in maintaining surface temperature and promoting vegetation activity. Under constant conditions, the photosynthetic capacity of vegetation increases with rising solar radiation [30,75]. Nonetheless, the SEM reveals that solar radiation's impact on the southern slope of the Tianshan Mountains contrasts with its effects on the northern slope and the Ili River Basin. This difference might stem from the correlation between vegetation coverage and the amount of solar radiation received, implying that areas with sparse vegetation engage in less photosynthesis. Despite higher levels of solar radiation, intense sunlight may lead to the closure of vegetation stomata, reducing or halting photosynthesis and adversely affecting grassland growth [76]. In contrast, areas with lush vegetation capture solar radiation fully, enhancing photosynthesis, increasing organic matter production [77], and fostering grassland development.

Moreover, the SEM underlines the significant impact of livestock numbers on grasslands in the Ili River Basin and the southern slopes of the Tianshan Mountains. Huang's study reports high grazing rates in the Ili River Basin [12], underscoring the region's reliance on animal husbandry. Mitigating this dependence through strategies like fenced breeding, planned grazing, and cultivating artificial grasslands is crucial. Although livestock can enhance soil nutrients and vegetation productivity, this benefit is confined mainly to a shift from light to moderate grazing intensity [75]. Thus, developing region-specific grazing policies is essential for improving the ecological health and vegetation productivity of pastoral areas. Human activities can either hasten or slow down the pace of ecosystem degradation or recovery, contingent upon natural factors [78]. Given Xinjiang's unique natural and geographical characteristics, population distribution varies significantly [79], with most regions characterized by low population densities and sensitive, fragile ecosystems. A moderate increase in population might support ecological projects and improve ecological quality. The structural equation model shows that the influence of nighttime light, indicative of human activity, on FVC is variable, suggesting that policy interventions can rapidly alter ecological conditions. Since the 1999 initiative to revert farmland to grassland, Xinjiang has implemented several ecological restoration projects, such as fencing and grassland enhancement, which have improved grassland conditions and broadly increased coverage [54]. While the ecological gains from these interventions may not equal the impacts of climate change, they have initiated positive changes in Xinjiang's regional environment, expanding forest and grassland areas, reducing natural disasters, and aiding in the restoration of grassland coverage and the overall ecological milieu.

4.3. Limitations and Future Work

This research provides critical insights into grassland FVC dynamics within the Xinjiang Tianshan Mountains and their interaction with environmental variables, yet it acknowledges certain constraints. Primarily, the GLASS dataset, despite offering a continuous spatiotemporal overview, suffers from a relatively broad resolution of 500 m. Secondly, the study did not take into account the influencing factors, such as soil pH [80], soil moisture [81], and weather extremes [82,83]. In addition, grassland vegetation exhibits a delayed response to environmental change, especially in the aspect of accumulated water shortage [84,85]. Ignoring these aspects will bring a certain degree of uncertainty to the research results. Therefore, in future studies, these limitations need to be further addressed through in-depth research and exploration to more accurately understand how the Xinjiang Tianshan grasslands respond to environmental changes.

5. Conclusions

This study utilized GLASS FVC data from 2001 to 2020 to investigate the spatiotemporal dynamics of grassland FVC in Xinjiang's Tianshan region, examining the effects of topography, seasonal temperature, precipitation, solar radiation, and changes in human activities (livestock numbers and nighttime light data) on FVC. Using SEM, both direct and indirect impacts were quantified. The main conclusions are as follows:

(1) Grasslands in the Tianshan region exhibit a spatial pattern of high central values surrounded by lower ones, with the highest FVC observed in the Ili River Basin. The FVC demonstrates a fluctuating upward trend, increasing at a rate of 0.0017 per year, with distinct periodic variations across sub-regions.
(2) The spatial trend of grassland FVC across the Tianshan Mountains shows a general improvement, with only 0.6% of the area experiencing severe degradation, primarily in the Ili River Basin. The Hurst index suggests that the persistence of grassland growth conditions in this region is weak, indicating potential degradation post-2020.
(3) SEM analysis indicates that the diversity of grassland vegetation in the Xinjiang Tianshan region is the result of complex interactions among topographical, climatic, and human factors. The region's topography acts as a natural barrier, accentuating environmental and urbanization differences between areas, which influence local key factors and thus, the distribution of FVC zones. Climatic factors, especially variations in precipitation and temperature, are critical in driving these spatial differences. In areas like the southern slope of the Tianshan Mountains and the Ili River Basin, where pastoralism is significant, a strong correlation exists between livestock numbers and grassland health.

Author Contributions: Conceptualization, Y.F. and X.Z.; data curation, Y.F., N.L. and W.Z.; formal analysis, Y.F., N.L. and W.S.; funding acquisition, X.Z.; methodology, Y.F., N.L. and W.Z.; resources, X.Z.; supervision, X.Z.; validation, Y.F., W.Z. and W.S.; visualization, Y.F. and N.L.; writing—original draft, Y.F.; writing—review and editing, Y.F., N.L. and X.Z. All authors have read and agreed to the published version of the manuscript.

Funding: This research was supported by the Third Xinjiang Scientific Expedition Program (Grant No. 2022xjkk0405).

Data Availability Statement: Datasets can be downloaded at the following links. The GLASS data are available at http://www.geodata.cn/ (accessed on 1 April 2023). The ERA5 reanalysis datasets are available at https://cds.climate.copernicus.eu/cdsapp (accessed on 9 April 2023). Population data can be obtained from https://www.worldpop.org/ (accessed on 16 April 2023). DEM data can be downloaded from https://cmr.earthdata.nasa.gov/search/concepts/C1546314043-LPDAAC_ECS.html (accessed on 1 April 2023). The land cover product MCD12Q1 V6 is available at https://developers.google.com/earth-engine/datasets/catalog/MODIS_006_MCD12Q1 (accessed on 3 April 2023).

Acknowledgments: We appreciate Beijing Normal University for providing the GLASS dataset, and the Public Data Portal for freely providing the dataset used in this study. We appreciate the National Earth System Science Data Center, National Science and Technology Infrastructure of China for providing the FVC data. We also thank the anonymous reviewers and editor for their valuable comments on the manuscript.

Conflicts of Interest: Author Naijing Liu was employed by POWERCHINA Northwest Engineering Corporation Limited. The remaining authors declare that the research was conducted in the absence of any commercial or financial relationships that could be construed as a potential conflict of interest.

Appendix A

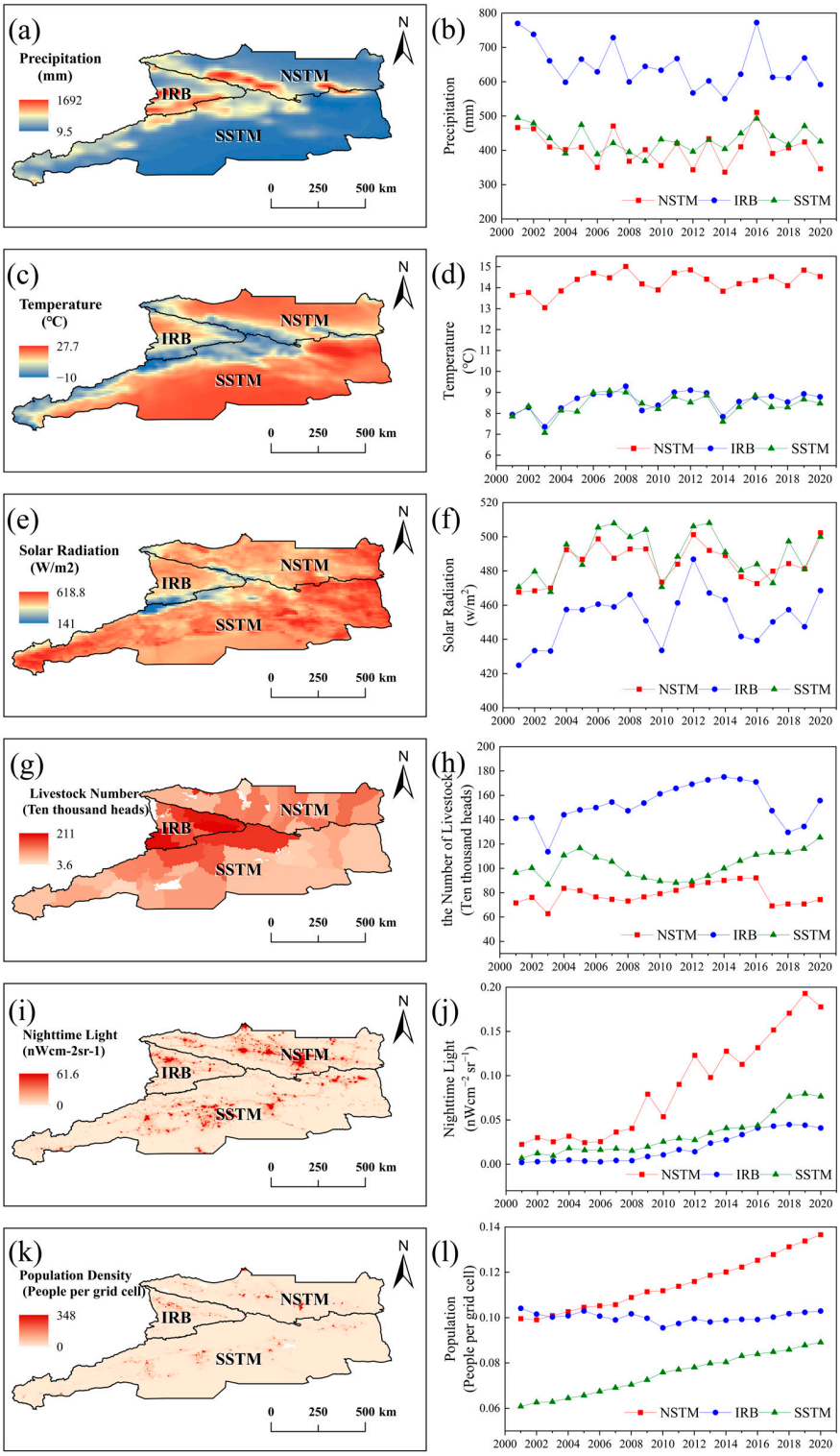

Figure A1. Spatial distribution of growing season accumulated precipitation (**a**), growing season mean annual temperature (**c**), growing season solar radiation (**e**), the number of livestock (**g**), nighttime light (**i**), population density (**k**), and interannual trends of growing season accumulated precipitation (**b**), growing season mean annual temperature (**d**), growing season solar radiation (**f**), the number of livestock (**h**), nighttime light (**j**), and population density (**l**) in different regions of the Tianshan Mountains region, Xinjiang, from 2001 to 2020.

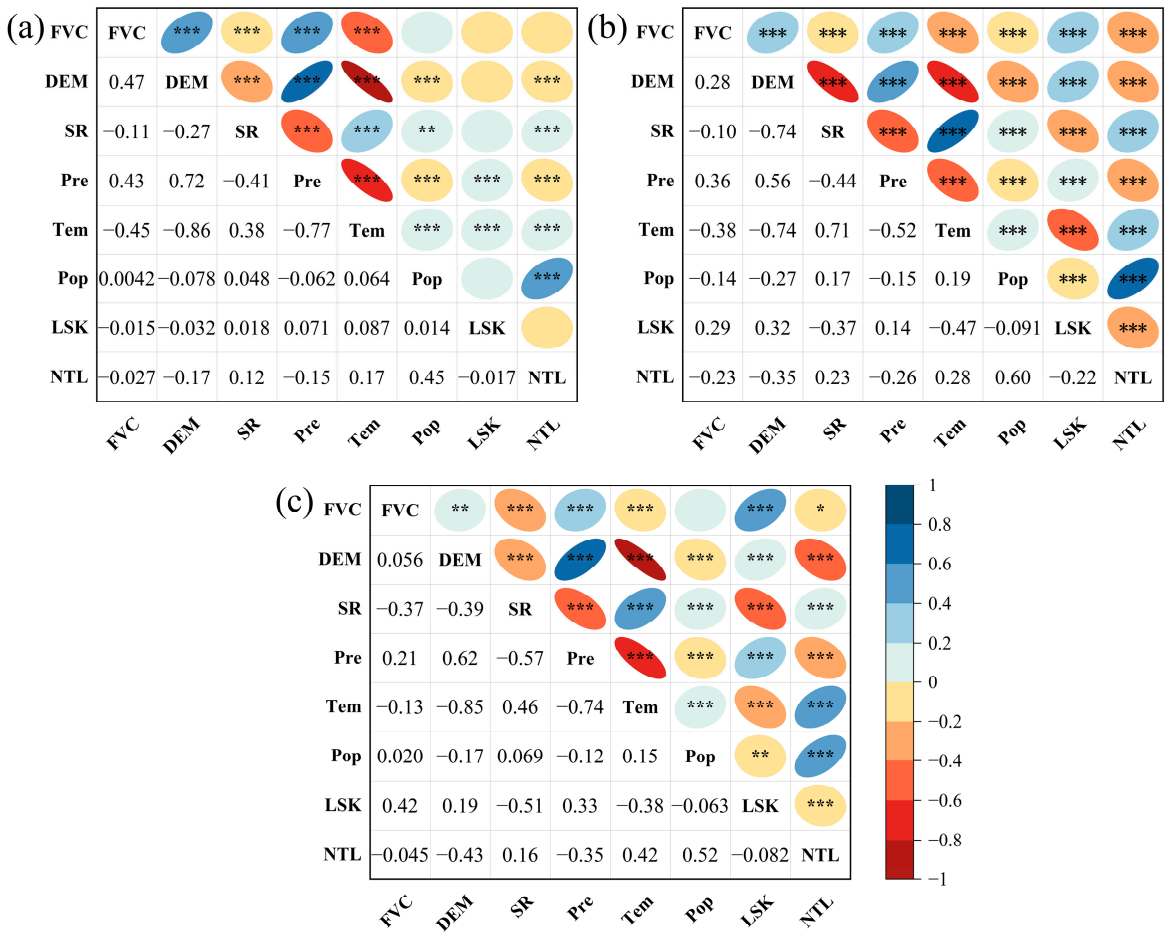

Figure A2. Correlations between FVC and topography, environmental factors, and human activities during the growing season in grasslands: (**a**) NSTM, (**b**) IRB, and (**c**) SSTM. Note: FVC denotes vegetation cover; DEM denotes elevation; SR denotes solar radiation; Pre denotes total precipitation; Tem denotes mean temperature; LSK denotes the number of livestock; NTL denotes nighttime light; and Pop denotes population density. Statistical significance: * means the significance level $p < 0.05$; ** means $p < 0.01$; *** means $p < 0.001$.

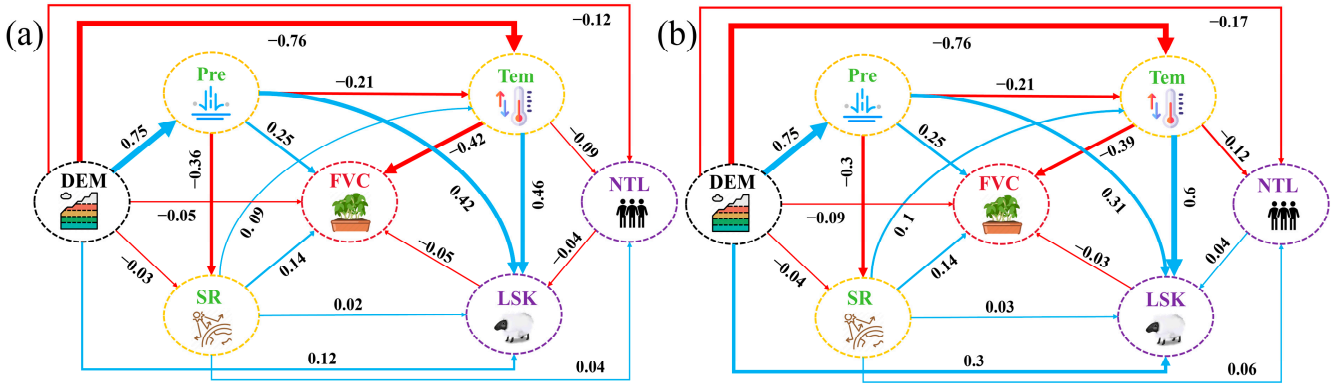

Figure A3. Structural equation model for the growing season of grasslands in the northern slope of the Tianshan Mountains: (**a**) 2001–2010; (**b**) 2011–2020. Abbreviations are the same as in Figure A2.

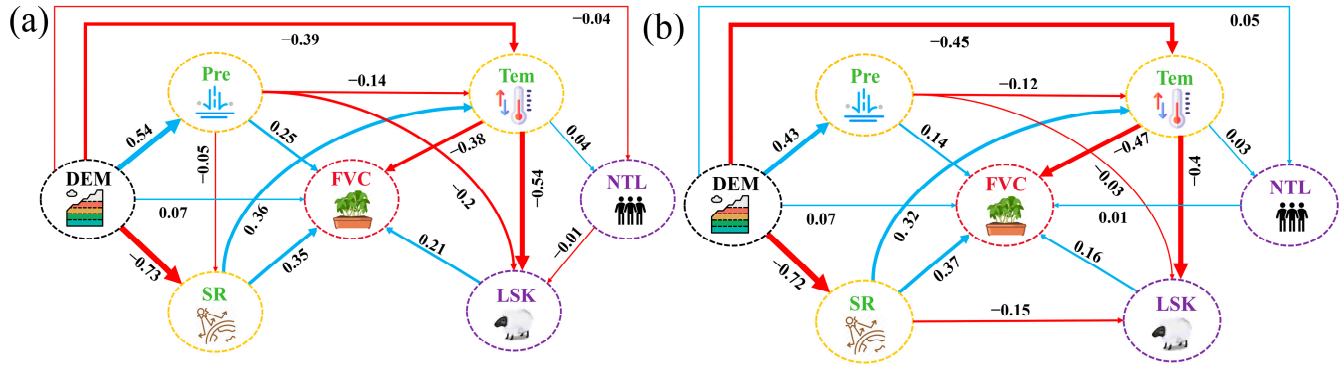

Figure A4. Structural equation model for the growing season of grasslands in the Ili River Basin: (**a**) 2001–2010; (**b**) 2011–2020. Abbreviations are the same as in Figure A2.

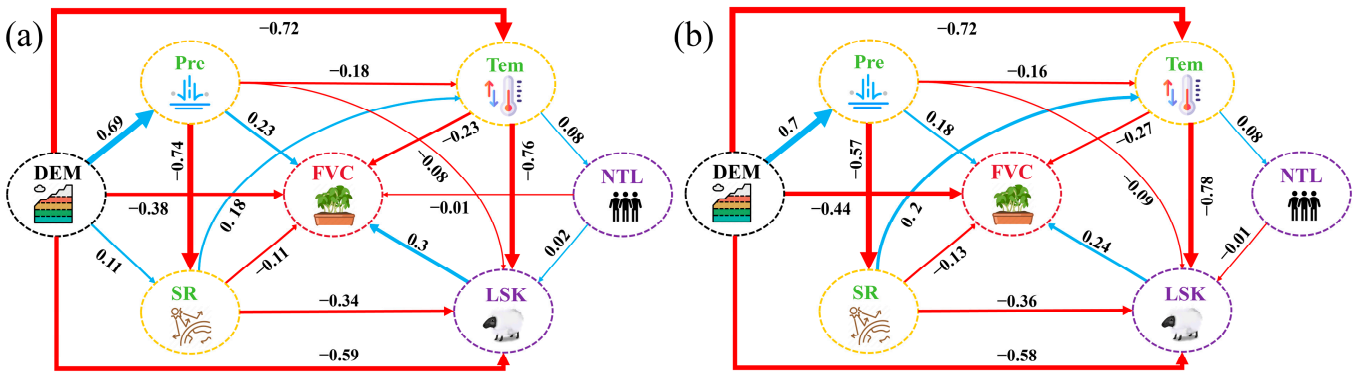

Figure A5. Structural equation model for the growing season of grasslands in the southern slope of Tianshan Mountains: (**a**) 2001–2010; (**b**) 2011–2020. Abbreviations are the same as in Figure A2.

References

1. Li, C.; Fu, B.; Wang, S.; Stringer, L.C.; Wang, Y.; Li, Z.; Liu, Y.; Zhou, W. Drivers and impacts of changes in China's drylands. *Nat. Rev. Earth Environ.* **2021**, *2*, 858–873. [CrossRef]
2. Liu, Y.; Wang, Q.; Zhang, Z.; Tong, L.; Wang, Z.; Li, J. Grassland dynamics in responses to climate variation and human activities in China from 2000 to 2013. *Sci. Total Environ.* **2019**, *690*, 27–39. [CrossRef]
3. Gao, G.Z.; Wang, M.L.; Li, D.H.; Li, N.N.; Wang, J.Y.; Niu, H.H.; Meng, M.; Liu, Y.; Zhang, G.H.; Jie, D.M. Phytolith evidence for changes in the vegetation diversity and cover of a grassland ecosystem in Northeast China since the mid-Holocene. *Catena* **2023**, *226*, 107061. [CrossRef]
4. Tans, P.P.; Fung, I.Y.; Takahashi, T. Observational constraints on the global atmospheric CO_2 budget. *Science* **1990**, *247*, 1431–1438. [CrossRef] [PubMed]
5. Gitelson, A.A.; Kaufman, Y.J.; Stark, R.; Rundquist, D. Novel algorithms for remote estimation of vegetation fraction. *Remote Sens. Environ.* **2002**, *80*, 76–87. [CrossRef]
6. Ma, R.; Zhang, J.Q.; Shen, X.J.; Liu, B.H.; Lu, X.G.; Jiang, M. Impacts of climate change on fractional vegetation coverage of temperate grasslands in China from 1982 to 2015. *J. Environ. Manag.* **2024**, *350*, 119694. [CrossRef]
7. Han, H.; Yin, Y.; Zhao, Y.; Qin, F. Spatiotemporal Variations in Fractional Vegetation Cover and Their Responses to Climatic Changes on the Qinghai-Tibet Plateau. *Remote Sens.* **2023**, *15*, 2662. [CrossRef]
8. Hussain, B.; Qureshi, N.A.; Buriro, R.A.; Qureshi, S.S.; Pirzado, A.A.; Saleh, T.A. Interdependence between temperature and precipitation: Modeling using copula method toward climate protection. *Model. Earth Syst. Environ.* **2022**, *8*, 2753–2766. [CrossRef]
9. Saleh, T.A. Protocols for synthesis of nanomaterials, polymers, and green materials as adsorbents for water treatment technologies. *Environ. Technol. Innov.* **2021**, *24*, 101821. [CrossRef]
10. Huang, H.; Xi, G.; Ji, F.; Liu, Y.; Wang, H.; Xie, Y. Spatial and Temporal Variation in Vegetation Cover and Its Response to Topography in the Selinco Region of the Qinghai-Tibet Plateau. *Remote Sens.* **2023**, *15*, 4101. [CrossRef]
11. Peng, D.L.; Zhang, B.; Wu, C.Y.; Huete, A.R.; Gonsamo, A.; Lei, L.P.; Ponce-Campos, G.E.; Liu, X.J.; Wu, Y.H. Country-level net primary production distribution and response to drought and land cover change. *Sci. Total Environ.* **2017**, *574*, 65–77. [CrossRef] [PubMed]
12. Huang, X.; Luo, G.; Ye, F.; Han, Q. Effects of grazing on net primary productivity, evapotranspiration and water use efficiency in the grasslands of Xinjiang, China. *J. Arid Land* **2018**, *10*, 588–600. [CrossRef]

13. Jiang, P.; Chen, D.; Xiao, J.; Liu, D.; Zhang, X.; Yang, X.; Ai, G. Climate and Anthropogenic Influences on the Spatiotemporal Change in Degraded Grassland in China. *Environ. Eng. Sci.* **2021**, *38*, 1065–1077. [CrossRef]
14. Ge, Y.; Wu, N.; Abuduwaili, J.; Issanova, G. Assessment of spatiotemporal features and potential sources of atmospheric aerosols over the Tianshan Mountains in arid central Asia. *Atmos. Environ.* **2023**, *294*, 119502. [CrossRef]
15. Song, Y.; Li, Y.; Cheng, L.; Zong, X.; Kang, S.; Ghafarpour, A.; Li, X.; Sun, H.; Fu, X.; Dong, J.; et al. Spatio-temporal distribution of Quaternary loess across Central Asia. *Palaeogeogr. Palaeoclimatol. Palaeoecol.* **2021**, *567*, 110279. [CrossRef]
16. Li, Y.; Chen, Y.; Sun, F.; Li, Z. Recent vegetation browning and its drivers on Tianshan Mountain, Central Asia. *Ecol. Indic.* **2021**, *129*, 107912. [CrossRef]
17. Liu, Q.; Yang, Z.; Han, F.; Wang, Z.; Wang, C. NDVI-based vegetation dynamics and their response to recent climate change: A case study in the Tianshan Mountains, China. *Environ. Earth Sci.* **2016**, *75*, 1189. [CrossRef]
18. Zhang, Y.; Liu, L.-Y.; Liu, Y.; Zhang, M.; An, C.-B. Response of altitudinal vegetation belts of the Tianshan Mountains in northwestern China to climate change during 1989–2015. *Sci. Rep.* **2021**, *11*, 4870. [CrossRef]
19. Yao, J.Q.; Chen, Y.N.; Zhao, Y.; Mao, W.Y.; Xu, X.B.; Liu, Y.; Yang, Q. Response of vegetation NDVI to climatic extremes in the arid region of Central Asia: A case study in Xinjiang, China. *Theor. Appl. Climatol.* **2018**, *131*, 1503–1515. [CrossRef]
20. Gao, Q.-Z.; Li, Y.; Xu, H.-M.; Wan, Y.-F.; Jiangcun, W.-Z. Adaptation strategies of climate variability impacts on alpine grassland ecosystems in Tibetan Plateau. *Mitig. Adapt. Strateg. Glob. Chang.* **2014**, *19*, 199–209. [CrossRef]
21. Ndehedehe, C.E.; Ferreira, V.G.; Agutu, N.O. Hydrological controls on surface vegetation dynamics over West and Central Africa. *Ecol. Indic.* **2019**, *103*, 494–508. [CrossRef]
22. Zhu, S.; Fang, X.; Hang, X.; Xie, X.; Sun, L.; Cao, L. Normalized difference vegetation index(NDVI)dynamics of grassland in Central Asia and its response to climate change and human activities. *J. Desert Res.* **2022**, *42*, 229–241.
23. Duan, Y.; Luo, M.; Guo, X.; Cai, P.; Li, F. Study on the Relationship between Snowmelt Runoff for Different Latitudes and Vegetation Growth Based on an Improved SWAT Model in Xinjiang, China. *Sustainability* **2021**, *13*, 1189. [CrossRef]
24. Cingolani, A.M.; Renison, D.; Tecco, P.A.; Gurvich, D.E.; Cabido, M. Predicting cover types in a mountain range with long evolutionary grazing history: A GIS approach. *J. Biogeogr.* **2008**, *35*, 538–551. [CrossRef]
25. Shang, Z.H.; Gibb, M.J.; Leiber, F.; Ismail, M.; Ding, L.M.; Guo, X.S.; Long, R.J. The sustainable development of grassland-livestock systems on the Tibetan plateau: Problems, strategies and prospects. *Rangel. J.* **2014**, *36*, 267–296. [CrossRef]
26. Bai, Y.; Xu, H.; Ling, H. Eco-service value evaluation based on eco-economic functional regionalization in a typical basin of northwest arid area, China. *Environ. Earth Sci.* **2014**, *71*, 3715–3726. [CrossRef]
27. Ostendorf, B.; Reynolds, J.F. A model of arctic tundra vegetation derived from topographic gradients. *Landsc. Ecol.* **1998**, *13*, 187–201. [CrossRef]
28. Wang, C.; Zhang, Z.; Zhang, J.; Tao, F.; Chen, Y.; Ding, H. The effect of terrain factors on rice production: A case study in Hunan Province. *J. Geogr. Sci.* **2019**, *29*, 287–305. [CrossRef]
29. Emran, A. Assessing topographic controls on vegetation characteristics in Chittagong Hill Tracts (CHT) from remotely sensed data (vol 11C, pg 198, 2018). *Remote Sens. Appl.-Soc. Environ.* **2018**, *11*, 198–208.
30. Gu, Z.N.; Zhang, Z.; Yang, J.H.; Wang, L.L. Quantifying the Influences of Driving Factors on Vegetation EVI Changes Using Structural Equation Model: A Case Study in Anhui Province, China. *Remote Sens.* **2022**, *14*, 4203. [CrossRef]
31. Lu, Y.; Zhao, J.; Qi, J.; Rong, T.; Wang, Z.; Yang, Z.; Han, F. Monitoring the Spatiotemporal Dynamics of Habitat Quality and Its Driving Factors Based on the Coupled NDVI-InVEST Model: A Case Study from the Tianshan Mountains in Xinjiang, China. *Land* **2022**, *11*, 1805. [CrossRef]
32. Li, L.-L.; Li, J.; Yu, R.-C. Evaluation of CMIP6 HighResMIP models in simulating precipitation over Central Asia. *Adv. Clim. Chang. Res.* **2022**, *13*, 1–13. [CrossRef]
33. Chen, C.; Jing, C.; Zhao, W.; Xu, Y. Grassland quality response to climate change in Xinjiang and predicted future trends. *Acta Prataculturae Sin.* **2022**, *31*, 1–16.
34. Yang, Z.; Xu, B. The concept and calculation method for comprehensive vegetation coverage of grasslands. *Pratacultural Sci.* **2019**, *36*, 1475–1478.
35. Zheng, W.; Zhu, J. Analysis of desertification process and driving force factors in grassland ecosystem of Xinjiang. *Pratacultural Sci.* **2012**, *29*, 1340–1351.
36. Zhang, K.; Wang, Y.; Mamtimin, A.; Liu, Y.Q.; Gao, J.C.; Aihaiti, A.; Wen, C.; Song, M.Q.; Yang, F.; Zhou, C.L.; et al. Temporal and Spatial Variations in Carbon Flux and Their Influencing Mechanisms on the Middle Tien Shan Region Grassland Ecosystem, China. *Remote Sens.* **2023**, *15*, 4091. [CrossRef]
37. Tang, Z.; Wang, X.; Wang, J.; Wang, X.; Li, H.; Jiang, Z. Spatiotemporal Variation of Snow Cover in Tianshan Mountains, Central Asia, Based on Cloud-Free MODIS Fractional Snow Cover Product, 2001–2015. *Remote Sens.* **2017**, *9*, 1045. [CrossRef]
38. Du, J.; Shu, J.; Yin, J.; Yuan, X.; Jiaerheng, A.; Xiong, S.; He, P.; Liu, W. Analysis on spatio-temporal trends and drivers in vegetation growth during recent decades in Xinjiang, China. *Int. J. Appl. Earth Obs. Geoinf.* **2015**, *38*, 216–228. [CrossRef]
39. Zhao, X.; Liang, S.L.; Liu, S.H.; Yuan, W.P.; Xiao, Z.Q.; Liu, Q.; Cheng, J.; Zhang, X.T.; Tang, H.R.; Zhang, X.; et al. The Global Land Surface Satellite (GLASS) Remote Sensing Data Processing System and Products. *Remote Sens.* **2013**, *5*, 2436. [CrossRef]
40. Meng, X.; Gao, X.; Li, S.; Lei, J. Spatial and Temporal Characteristics of Vegetation NDVI Changes and the Driving Forces in Mongolia during 1982–2015. *Remote Sens.* **2020**, *12*, 603. [CrossRef]

41. Jiao, D.; Xu, N.; Yang, F.; Xu, K. Evaluation of spatial-temporal variation performance of ERA5 precipitation data in China. *Sci. Rep.* **2021**, *11*, 17956. [CrossRef] [PubMed]
42. Chen, Z.; Yu, B.; Yang, C.; Zhou, Y.; Yao, S.; Qian, X.; Wang, C.; Wu, B.; Wu, J. An extended time series (2000–2018) of global NPP-VIIRS-like nighttime light data from a cross-sensor calibration. *Earth Syst. Sci. Data* **2021**, *13*, 889–906. [CrossRef]
43. Sen, P.K. Estimates of the regression coefficient based on Kendall's tau. *J. Am. Stat. Assoc.* **1968**, *63*, 1379–1389. [CrossRef]
44. Theil, H. A rank-invariant method of linear and polynomial regression analysis. In *Henri Theil's Contributions to Economics and Econometrics: Econometric Theory and Methodology*; Springer: Berlin/Heidelberg, Germany, 1992; pp. 345–381.
45. Jiang, F.; Deng, M.; Long, Y.; Sun, H. Spatial Pattern and Dynamic Change of Vegetation Greenness From 2001 to 2020 in Tibet, China. *Front. Plant Sci.* **2022**, *13*, 892625. [CrossRef] [PubMed]
46. Mann, H.B. Nonparametric tests against trend. *Econometrica* **1945**, *13*, 245–259. [CrossRef]
47. Kendall, M.G. Rank Correlation Methods. 1948. Available online: https://psycnet.apa.org/record/1948-15040-000 (accessed on 6 April 2023).
48. Ranjan, A.K.; Parida, B.R.; Dash, J.; Gorai, A.K. Quantifying the impacts of opencast mining on vegetation dynamics over eastern India using the long-term Landsat-series satellite dataset. *Ecol. Inform.* **2022**, *71*, 101812. [CrossRef]
49. Hurst, H.E. Long-Term Storage Capacity of Reservoirs. *Trans. Am. Soc. Civ. Eng.* **1951**, *116*, 770–799. [CrossRef]
50. Liu, C.X.; Zhang, X.D.; Wang, T.; Chen, G.Z.; Zhu, K.; Wang, Q.; Wang, J. Detection of vegetation coverage changes in the Yellow River Basin from 2003 to 2020. *Ecol. Indic.* **2022**, *138*, 108818. [CrossRef]
51. Hao, J.; Xu, G.; Luo, L.; Zhang, Z.; Yang, H.; Li, H. Quantifying the relative contribution of natural and human factors to vegetation coverage variation in coastal wetlands in China. *Catena* **2020**, *188*, 104429. [CrossRef]
52. Shao, W.; Wang, Q.; Guan, Q.; Luo, H.; Ma, Y.; Zhang, J. Distribution of soil available nutrients and their response to environmental factors based on path analysis model in arid and semi-arid area of northwest China. *Sci. Total Environ.* **2022**, *827*, 154254. [CrossRef]
53. Zheng, H.; Miao, C.; Li, X.; Kong, D.; Gou, J.; Wu, J.; Zhang, S. Effects of Vegetation Changes and Multiple Environmental Factors on Evapotranspiration Across China Over the Past 34 Years. *Earths Future* **2022**, *10*, e2021EF002564. [CrossRef]
54. Zhao, W.K.; Jing, C.Q. Response of the natural grassland vegetation change to meteorological drought in Xinjiang from 1982 to 2015. *Front. Environ. Sci.* **2022**, *10*, 1047818. [CrossRef]
55. Ke, C.-Q.; Liu, X. MODIS-observed spatial and temporal variation in snow cover in Xinjiang, China. *Clim. Res.* **2014**, *59*, 15–26. [CrossRef]
56. Aisikeer, Y.; Rusuli, Y. Spatiotemporal variation characteristics and trend analysis of vegetation and water area in the Bosten Lake based on multiple endmember spectral mixture analysis model. *Arid Land Geogr.* **2023**, *46*, 1622–1631.
57. Amuti, T.; Luo, G. Analysis of land cover change and its driving forces in a desert oasis landscape of Xinjiang, northwest China. *Solid Earth* **2014**, *5*, 1071–1085. [CrossRef]
58. He, P.; Sun, Z.; Han, Z.; Dong, Y.; Liu, H.; Meng, X.; Ma, J. Dynamic characteristics and driving factors of vegetation greenness under changing environments in Xinjiang, China. *Environ. Sci. Pollut. Res.* **2021**, *28*, 42516–42532. [CrossRef] [PubMed]
59. Qin, G.; Lu, Q.; Meng, Z.; Li, Z.; Chen, H.; Kong, J.; Ji, Z.; Qin, A. Spatial-temporal Dynamics of Grassland NDVI and Its Response to Climate Change in Northern China from 1982 to 2015. *Res. Soil Water Conserv.* **2021**, *28*, 101–108, 117.
60. Yong, Z.; Fahu, C.; Xiaohua, G.O.U.; Linya, J.I.N.; Qinhua, T.; Yousheng, W.; Jianfeng, P. The Temporal and Spatial Distribution of Seasonal Dry-Wet Changes over the Northwestern China: Based on PDSI. *Acta Geogr. Sin.* **2007**, *62*, 1142–1152.
61. Yao, J.; Chen, J.; Dilinuer, T.; Han, X.; Mao, W. Trend of climate and hydrology change in Xinjiang and its problems thinking. *J. Glaciol. Geocryol.* **2021**, *43*, 1498–1511.
62. Zhang, R.P.; Guo, J.; Yin, G. Response of net primary productivity to grassland phenological changes in Xinjiang, China. *Peerj* **2021**, *9*, 10650. [CrossRef]
63. Horion, S.; Cornet, Y.; Erpicum, M.; Tychon, B. Studying interactions between climate variability and vegetation dynamic using a phenology based approach. *Int. J. Appl. Earth Obs. Geoinf.* **2013**, *20*, 20–32. [CrossRef]
64. He, C.; Tian, J.; Gao, B.; Zhao, Y. Differentiating climate- and human-induced drivers of grassland degradation in the Liao River Basin, China. *Environ. Monit. Assess.* **2015**, *187*, 4199. [CrossRef]
65. Liu, Y.; Li, L.; Chen, X.; Zhang, R.; Yang, J. Temporal-spatial variations and influencing factors of vegetation cover in Xinjiang from 1982 to 2013 based on GIMMS-NDVI$_{3g}$. *Glob. Planet. Chang.* **2018**, *169*, 145–155. [CrossRef]
66. Li, Z.; Chen, Y.; Fang, G.; Li, Y. Multivariate assessment and attribution of droughts in Central Asia. *Sci. Rep.* **2017**, *7*, 1316. [CrossRef] [PubMed]
67. Tang, Q.; Liu, X.; Zhou, Y.; Wang, P.; Li, Z.; Hao, Z.; Liu, S.; Zhao, G.; Zhu, B.; He, X.; et al. Climate change and water security in the northern slope of the Tianshan Mountains. *Geogr. Sustain.* **2022**, *3*, 246–257. [CrossRef]
68. Wang, X.; Liu, L.; Piao, S.; Janssens, I.A.; Tang, J.; Liu, W.; Chi, Y.; Wang, J.; Xu, S. Soil respiration under climate warming: Differential response of heterotrophic and autotrophic respiration. *Glob. Chang. Biol.* **2014**, *20*, 3229–3237. [CrossRef] [PubMed]
69. Xun, Q.; An, S.; Lu, M. Climate change and topographic differences influence grassland vegetation greening across environmental gradients. *Front. Environ. Sci.* **2024**, *11*, 1324742. [CrossRef]
70. Han, W.; Guan, J.; Zheng, J.; Liu, Y.; Ju, X.; Liu, L.; Li, J.; Mao, X.; Li, C. Probabilistic assessment of drought stress vulnerability in grasslands of Xinjiang, China. *Front. Plant Sci.* **2023**, *14*, 1143863. [CrossRef]

71. He, X.; Zhang, F.; Cai, Y.; Tan, M.L.; Chan, N.W. Spatio-temporal changes in fractional vegetation cover and the driving forces during 2001-2020 in the northern slopes of the Tianshan Mountains, China. *Environ. Sci. Pollut. Res.* **2023**, *30*, 75511–75531. [CrossRef] [PubMed]
72. Dai, L.; Li, Y.; Luo, G.; Xu, W.; Lu, L.; Li, C.; Feng, Y. The spatial variation of alpine timberlines and their biogeographical characteristics in the northern Tianshan Mountains of China. *Environ. Earth Sci.* **2013**, *68*, 129–137. [CrossRef]
73. Schiemann, R.; Luethi, D.; Vidale, P.L.; Schaer, C. The precipitation climate of Central Asia—Intercomparison of observational and numerical data sources in a remote semiarid region. *Int. J. Climatol.* **2008**, *28*, 295–314. [CrossRef]
74. Sun, G.; Chen, Y.; Li, W.; Pan, C.; Li, J.; Yang, Y. Spatial distribution of the extreme hydrological events in Xinjiang, north-west of China. *Nat. Hazards* **2013**, *67*, 483–495. [CrossRef]
75. Ge, W.; Deng, L.; Wang, F.; Han, J. Quantifying the contributions of human activities and climate change to vegetation net primary productivity dynamics in China from 2001 to 2016. *Sci. Total Environ.* **2021**, *773*, 145648. [CrossRef] [PubMed]
76. Baligar, V.C.; Elson, M.K.; He, Z.; Li, Y.; Paiva, A.d.Q.; Almeida, A.A.F.; Ahnert, D. Light Intensity Effects on the Growth, Physiological and Nutritional Parameters of Tropical Perennial Legume Cover Crops. *Agronomy* **2020**, *10*, 1515. [CrossRef]
77. Shi, Y.; Xu, L.; Zhou, Y.; Ji, B.; Zhou, G.; Fang, H.; Yin, J.; Deng, X. Quantifying driving factors of vegetation carbon stocks of Moso bamboo forests using machine learning algorithm combined with structural equation model. *For. Ecol. Manag.* **2018**, *429*, 406–413. [CrossRef]
78. Zhang, R.; Liang, T.; Guo, J.; Xie, H.; Feng, Q.; Aimaiti, Y. Grassland dynamics in response to climate change and human activities in Xinjiang from 2000 to 2014. *Sci. Rep.* **2019**, *9*, 2888. [CrossRef] [PubMed]
79. Chang, Y.; Li, D.B.; Simayi, Z.; Ren, Y.W.; Yang, S.T. Spatial Distribution of Leisure Agriculture in Xinjiang and Its Influencing Factors Based on Geographically Weighted Regression. *Sustainability* **2022**, *14*, 5002. [CrossRef]
80. Liu, K.; Liu, Z.; Zhou, N.; Shi, X.; Lock, T.R.; Kallenbach, R.L.; Yuan, Z. Predicted increased P relative to N growth limitation of dry grasslands under soil acidification and alkalinization is ameliorated by increased precipitation. *Soil Biol. Biochem.* **2022**, *173*, 108812. [CrossRef]
81. Zhang, H.; Kattel, G.R.; Wang, G.; Chuai, X.; Zhang, Y.; Miao, L. Enhanced soil moisture improves vegetation growth in an arid grassland of Inner Mongolia Autonomous Region, China. *J. Arid Land* **2023**, *15*, 871–885. [CrossRef]
82. Girardin, M.P.; Hogg, E.H.; Bernier, P.Y.; Kurz, W.A.; Guo, X.J.; Cyr, G. Negative impacts of high temperatures on growth of black spruce forests intensify with the anticipated climate warming. *Glob. Chang. Biol.* **2016**, *22*, 627–643. [CrossRef]
83. Li, C.; Leal Filho, W.; Yin, J.; Hu, R.; Wang, J.; Yang, C.; Yin, S.; Bao, Y.; Ayal, D.Y. Assessing vegetation response to multi-time-scale drought across inner Mongolia plateau. *J. Clean. Prod.* **2018**, *179*, 210–216. [CrossRef]
84. Zhang, Z.; Ju, W.; Zhou, Y.; Li, X. Revisiting the cumulative effects of drought on global gross primary productivity based on new long-term series data (1982–2018). *Glob. Chang. Biol.* **2022**, *28*, 3620–3635. [CrossRef] [PubMed]
85. Zhao, A.; Yu, Q.; Feng, L.; Zhang, A.; Pei, T. Evaluating the cumulative and time-lag effects of drought on grassland vegetation: A case study in the Chinese Loess Plateau. *J. Environ. Manag.* **2020**, *261*, 110214. [CrossRef] [PubMed]